Gasoline from the bioliq® process: Production, characterization and performance

Tobias Michler[a,*], Nicolas Wippermann[a], Olaf Toedter[a], Benjamin Niethammer[b], Thomas Otto[b], Ulrich Arnold[b], Stephan Pitter[b], Thomas Koch[a], Jörg Sauer[b]

[a] Karlsruhe Institute of Technology (KIT), Institute of Internal Combustion Engines (IFKM), Rintheimer Querallee 2, 76131 Karlsruhe, Germany
[b] Karlsruhe Institute of Technology (KIT), Institute of Catalysis Research and Technology (IKFT), Hermann-von-Helmholtz-Platz 1, 76344 Eggenstein-Leopoldshafen, Germany

Keywords:
Combustion efficiency
Particle size distribution
Soot reactivity
Biofuels synthesis
Catalytic fuel synthesis
Biofuels

A B S T R A C T

Within the so-called bioliq® process, renewable carbon resources, especially agricultural residues, are converted to gasoline. The process chain comprises pyrolysis of the feedstocks, gasification to synthesis gas, gas cleaning and conversion of synthesis gas to dimethyl ether (DME) followed by conversion of DME to hydrocarbons. Construction of all process units has been completed now and the entire plant has been successfully operated in several campaigns. Thus, hundreds of liters of a new alternative gasoline are available now, which allow for an extensive testing. The basic characteristics of the resulting bioliq®/100 fuel are described. It is rich in aromatics and a blend consisting of 90 Vol. % of conventional RON95 E5 fuel and 10 Vol. % of bioliq®/100, designated as bioliq®/10, has been produced which meets the DIN EN 228 standard. Initial measurements on a single cylinder research engine have been carried out focusing on efficiency and emissions. A comparison of bioliq®/10 with neat RON95 E5 revealed an improved knocking behavior of bioliq®/10 even by a small fraction of regenerative bioliq® fuel. Particle as well as hydrocarbon emissions from bioliq®/10 are significantly higher than in the case of RON95 E5. Increased particle emissions are attributed to the higher content of aromatics. Soot reactivity has been investigated and soot from bioliq®/10 exhibits higher reactivity than soot from RON95 E5.

1. Introduction

With the indispensable demand for CO_2 neutral mobility, the development of greenhouse gas neutral fuels is required in addition to the establishment of an electric vehicle fleet. Both strategies are needed to achieve the national climate targets and climate targets of the European Union. The main target is a reduction of greenhouse gases from anthropogenic sources by 40% until 2030, compared to 1990, and the long term plan is a reduction of greenhouse gases by 80 95% until 2050 [1,2].

In addition to the limitation of greenhouse gas emissions, increasingly strict exhaust gas emission standards are being adopted. With the EURO 6b standard, for gasoline engines, not only gaseous emissions like carbon monoxide (CO), hydrocarbons (HC) and nitrogen oxides (NO_x) are regulated but also particulate matter (PM). Thus, the particle number (PN) is restricted to 6×10^{11} #/cm^3 because of the proven health impacts of such particles [3 5]. Restriction of the PN forces the manufacturers to equip gasoline engines, especially engines with direct injection (DI) [6], with gasoline particle filters (GPF) [7]. In this context, new fuels which enable clean combustion with significantly reduced particle emissions are likewise desirable. In addition, a facile regeneration of the GPF should be possible even in the case of low soot loads. Thus, the soot filtered by the GPF should exhibit a high reactivity to prevent overheating of the GPF and a high exhaust back pressure of the engine.

Regarding the development of new CO_2 neutral fuels, major challenges are the availability of renewable feedstocks, sustainable production and sufficient performance. The latter criterion strongly depends on physical chemical and combustion properties. For instance, heating values should be high to minimize fuel consumption and high research octane numbers (RON) are needed to guarantee high knocking resistance and durability of the engines. Regarding the former criteria, two main approaches for the sustainable synthesis of hydrocarbon fuels are currently explored. On the one hand, strategies for the valorization of CO_2, e.g. by reduction with hydrogen, are investigated and on the other hand strategies for converting renewable biomass to fuels are further developed [8]. A prominent example for the latter pathway is the generation of synthesis gas from biomass, e.g. agricultural residues.

* Corresponding author.
E-mail addresses: tobias.michler@kit.edu (T. Michler), olaf.toedter@kit.edu (O. Toedter), thomas.otto@kit.edu (T. Otto), ulrich.arnold@kit.edu (U. Arnold).

In the next step, synthesis gas can be further processed to a series of valuable fuels such as hydrocarbons via the Fischer Tropsch reaction or methanol and methanol based fuels [9]. Another option, which is described here, is the direct synthesis of dimethyl ether (DME) from synthesis gas followed by DME conversion to hydrocarbons [10]. The procedure is closely related to methanol based processes, especially Methanol To Gasoline (MTG) processes, and feasibility has been demonstrated in several studies which are summarized in [11]. However, demonstration of the entire process chain from feedstocks to fuels and significantly above laboratory scale is still fragmentary and recent progress in this field, including engine tests, is presented here.

Within this work, a blend of customary RON95 E5 fuel with a new fuel produced from regenerative biomass has been investigated. The fuel is a product of the bioliq® process which is operated at the Karlsruhe Institute of Technology (KIT). The process and the basic characteristics of the resulting bioliq®/100 fuel are described. The blend comprises 90 Vol.−% RON95 E5 and 10 Vol.−% bioliq®/100, hereinafter referred to as bioliq®/10. It meets the DIN EN 228 standard and can be tested directly, i.e. without significant modification of the test engine. Thus, initial measurements on a single cylinder research engine have been carried out focusing on knock limit, thermodynamic parameters (i.e. start of combustion), particle size distribution (PSD) and total particle number concentration (TPNC), soot reactivity and hydrocarbon (HC) emissions.

Major objectives of this study are

- to give a compact overview of the key features of the bioliq® process, to determine basic properties of both, the pure bioliq® fuel and a blend with conventional gasoline,
- and to identify important combustion characteristics.

Thus, a comprehensive evaluation is envisaged considering fuel production as well as fuel performance.

2. Fuel production and properties

2.1. The bioliq® process

The intention of the bioliq® process is the conversion of residual biomass to high quality gasoline. The bioliq® pilot plant at KIT was constructed between 2005 and 2013 and initial operation of the entire process chain was launched in 2014 [12 14]. The bioliq® process comprises four steps (Fig. 1). Straw is used as starting material. In the first step, the energy density of the biomass is increased by fast pyrolysis [15 17]. Thereby, a liquid intermediate fuel, called biosyncrude®, is formed. The biosyncrude® is then processed into a mixture of CO and H_2 (synthesis gas) with a low methane content and free of tar, employing high pressure entrained flow gasification [18 20]. Subsequently, acidic gases and impurities are removed from the hot syngas in a cleaning step. Particulates are removed in a ceramic hot gas filter unit. A two stage fixed bed sorption retains acidic gases like HCl, H_2S, COS and alkali. Mineral sorbents and a catalytic converter decompose ammonia, HCN, and organic trace compounds. The process chain is completed by single stage DME synthesis [21 23], followed by conversion to gasoline in a DME To Gasoline (DTG) process [24 26].

A flow diagram of the bioliq® process steps IIIb and IV is shown in Fig. 2. The synthesis gas is directly converted to DME (process step IIIb) and for this purpose, the CO:H_2 ratio is adjusted to 1:1 employing the water gas shift reaction and CO_2 absorption. Then, the raw product stream from the DME reactor is converted to gasoline via the DTG reaction (process step IV). The resulting product spectrum comprises light hydrocarbons, a mixture of paraffinic, olefinic, naphthenic and aromatic hydrocarbons in the boiling range of gasoline and water as by product. After gasoline synthesis, water and light hydrocarbons are separated from the raw gasoline product, which is subsequently transferred to a rectification column and purified by distillation. Regarding the scale of fuel production, the pyrolysis step is designed for an input of about 500 kg/h of air dried biomass. From the gasifier, 700 Nm^3/h are separated from the raw gas stream resulting in a nominal capacity of the synthesis plant of about 100 L gasoline/h.

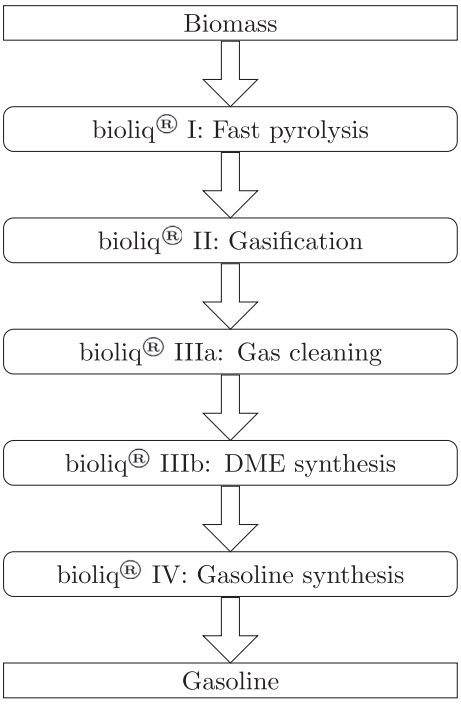

Fig. 1. Conversion steps in the bioliq® process.

2.2. Fuel characteristics

The bio based gasoline from the bioliq® plant (bioliq® campaign November 2017) was taken from the middle of a rectification column (Fig. 2) and is called bioliq®/100 in the following. Analysis of the bioliq®/100 gasoline was carried out via gas chromatography according to the ASTM D6730 01 (2016) standard. The product spectrum exhibits a high content of C_7 to C_{10} aromatics wherein C_8 aromatics are dominating (Fig. 3).

The distillation curve of the bioliq®/100 gasoline (Fig. 4) reveals a fraction of high boiling components (about 5 Vol.−% in addition to evaporation residue). In order to remove this fraction, bioliq®/100 was distilled batchwise on laboratory scale up to a temperature of 210 °C, at atmospheric pressure. A residue amounting to 5 Vol.−% remained as the bottom product and some of the light hydrocarbons ($< C_6$) were discharged. The mass fractions of the compound classes with a content above 1 wt.−% are shown in Fig. 3. Regarding oxygenates, only methanol could be detected in the raw gasoline. The content is around 2% and it is completely removed after distillation. It can be seen that C_9 aromatics have been partially removed while C_{10} and higher components have been completely removed. The resulting hydrocarbon mixture contains about 75 wt.−% of aromatics.

This mixture is completely miscible with conventional RON95 E5 gasoline up to a proportion of 10 Vol.−%. Analogous blends (10 Vol.−% distilled bioliq®/100 + 90 Vol.−% RON95 E5, called bioliq®/10 in the following) have been investigated within this work, in comparison with commercial RON95 E5 gasoline. Fig. 4 shows the distillation curves of RON95 E5 and the corresponding bioliq®/10 gasoline. The curves are nearly identical, except for the low boiling area, where the curve of bioliq®/10 is slightly below the curve of RON95 E5 and in the middle temperature range, where it is slightly above. For comparison, the distillation curve of bioliq®/100 is also shown.

Table 1 shows that the bioliq®/10 is within the relevant criteria of

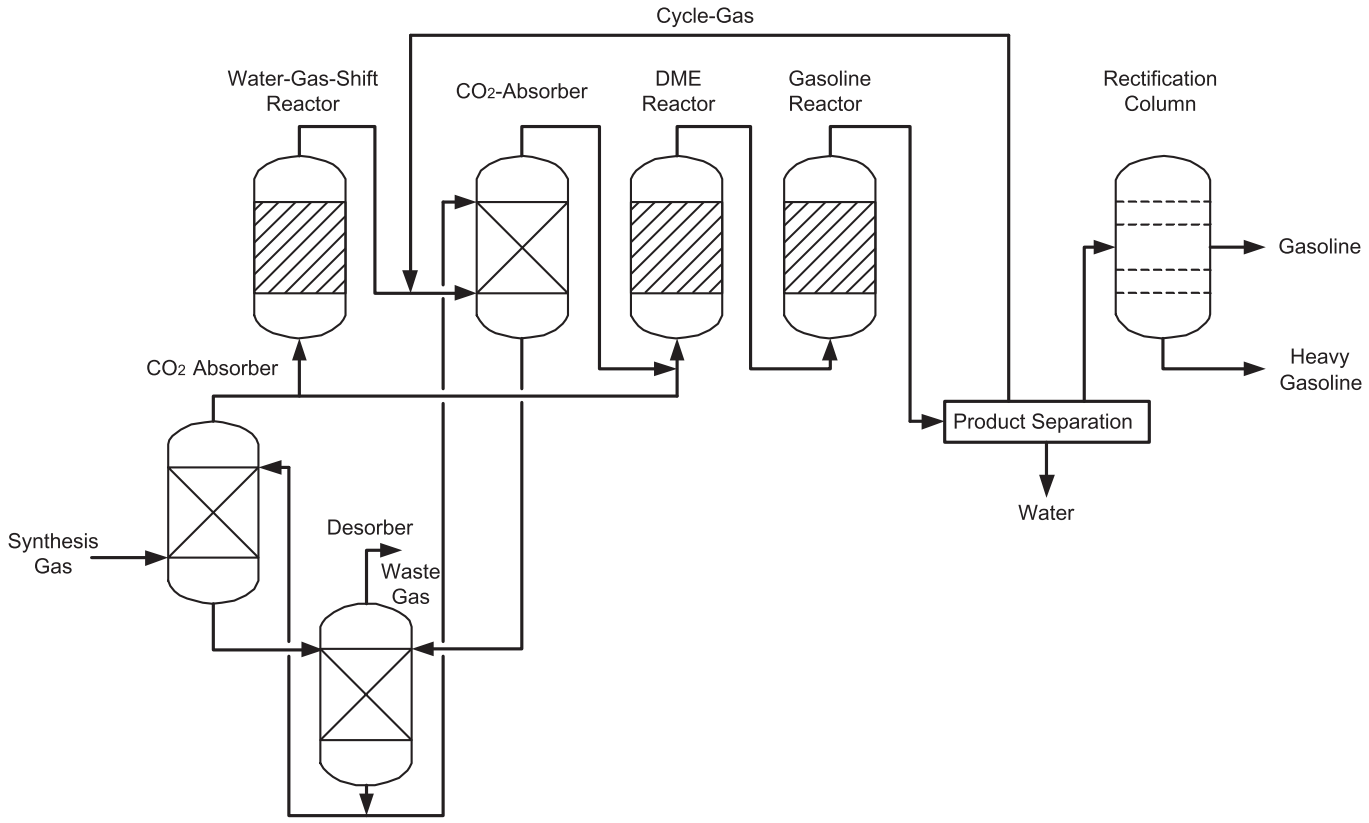

Fig. 2. Flow diagram of the bioliq® steps IIIb and IV.

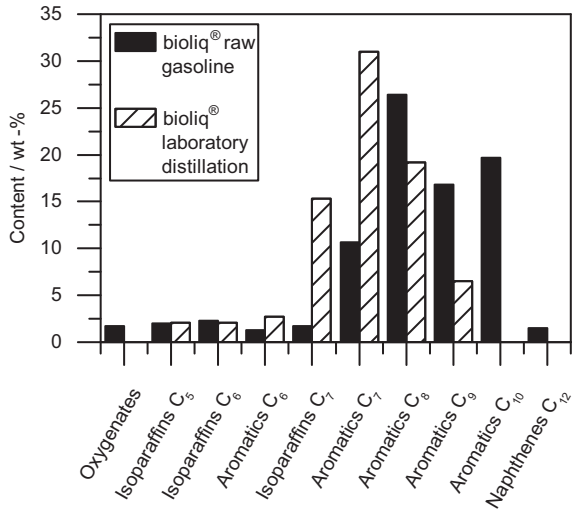

Fig. 3. Composition of bioliq®/100 gasoline and the corresponding laboratory distillate, measured according to ASTM D6730-01 (2016). Only compound classes with a content above 1 wt. % are shown.

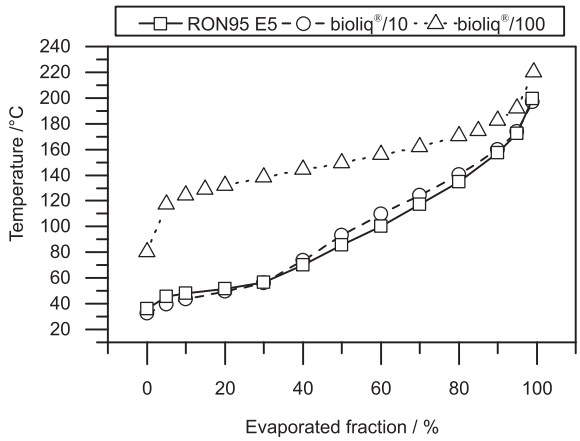

Fig. 4. Distillation curves of RON95 E5, bioliq®/10 and bioliq®/100 according to [27].

the DIN EN 228 standard for automotive fuels. Its molecular composition is in good accordance with conventional RON95 E5 gasoline. The density at 15 °C is in the range of requirements of the DIN EN 228 standard and the lower heating value does not differ from the reference gasoline. Likewise, the high aromatics content of the bioliq®/10 gasoline does not exceed the maximum value of the DIN EN 228 [28] standard.

3. Experimental setup

The experimental setup is subdivided into two parts, the used measurement devices and the engine setup, which are described separately in the following.

3.1. Measurement setup

The engine is equipped with two piezo resistive low pressure sensors (4045 and 4075) at the inlet and outlet as well as a high pressure sensor (6054AR) from Kistler for recording the thermodynamic measurement variables. The in cylinder pressure is recorded by a data acquisition system (DEWETRON DEWE800). Depending on the crank angle encoder, the measurement frequency is 0.1° crank angle (CA). The inflowing air mass is measured by a mass air flow meter from Sensycon. For measuring the fuel consumption (in kg $\times$ h^{-1}), a Krohne MFM7050 Coriolis flow meter is used. The air fuel ratio (AF) is

Table 1
Comparison of the fuel characteristics of RON95 E5 and bioliq®/10.

Property	RON95 E5	bioliq®/10	DIN EN 228
Molecular formula	$C_{6.8}H_{13.0}O_{0.13}$	$C_{6.9}H_{12.8}O_{0.11}$	–
Density at 15 °C/kg∗m ^{3}	740.6	747.0	720–775
Vapor pressure (DVPE)/kPa	63.8	74.1	60–90
Lower heating value/MJ∗kg ^{1}	42.39	42.39	–
RON	95.6	96.4	min. 95
MON	85.5	85.5	min. 85
Air demand/kg∗kg ^{1}	14.29	14.29	–
Aromatics content/Vol. %	28.9	33.0	max. 35
Benzene/Vol. %	0.92	0.95	1.0
Toluene/Vol. %	7.1	7.8	–
Ethylbenzene/Vol. %	1.6	1.5	–
p-Xylene/Vol. %	1.9	2.1	–
m-Xylene/Vol. %	3.8	4.8	–
o-Xylene/Vol. %	2.0	2.4	–
iso-Propylbenzene/Vol. %	0.2	0.2	–
n-Propylbenzene/Vol. %	0.4	0.4	–
1,3- & 1,4-Ethylmethylbenzene/Vol. %	2.1	2.4	–
1,2-Ethylmethylbenzene/Vol. %	0.5	0.6	–
1,3,5-Trimethylbenzene/Vol. %	0.7	0.9	–
1,2,4-Trimethylbenzene/Vol. %	2.5	3.1	–
1,2,3-Trimethylbenzene/Vol. %	0.5	0.8	–
Sum C_8 aromatics/Vol. %	9.3	10.9	–
Sum C_9 aromatics/Vol. %	6.9	8.4	–
Sum C_{10} or higher aromatics/Vol. %	4.8	5.0	–
Methyl tertiary-butyl ether	< 0.1	< 0.1	22.0
Ethanol	4.8	4.5	10

determined by two lambda sensors and lambda meters (ETAS LA4). The sampled exhaust gas is led to an AVL AMA4000 flame ionization de tector (FID) via a heated sample line and measurements are carried out standalone for hydrocarbons (HC) using C_3H_8 for calibration of the FID.

Additionally to the gaseous HC emissions the total particle number concentration (TPNC), the particle size distribution (PSD) and the soot reactivity is determined. The TPNC and the PSD is measured by a Model 3090 Engine Exhaust Particle Sizer (EEPS) from TSI. This sizer has a measurement range of particle diameters from 5.6 to 560 nm at 32 classes. The sampled aerosol is charged by a unipolar charger and led with sheath air to the electrometer column, which is shown in the right picture of Fig. 5. At the outer part of the device, 22 electrometers de termine the impaction of particles. The 'electrical mobility' diameter of the particles is determined by the position of the particles hitting the electrometer. This position depends on the charge of the particles. The electrometers measure the charge transferred by the particles to count the particles. The measured PSD is then converted by a so called in version matrix. In this publication the 'soot' matrix, presented in [29], for non spherical particles is used as recommended by [30]. The mea surement setup for the PSD, TPNC, and gaseous emissions is shown in the left picture of Fig. 5. To sample the aerosol from the exhaust pipe, a borehole probe with a sampling pipe of approximately 0.4 m length is used. The probe is positioned 0.5 m after a reservoir. The pipe is con nected to the first dilution by a Matter Engineering MDE19 E rotation disk diluter [31]. The dilution factor and the temperature of the dilu tion head are set to 16.5 and 120 °C, respectively. Through a 3 m un heated sample line the aerosol is led to an evaporation tube with diluter [31]. In this tube the aerosol is heated up to 300 °C and then diluted with a dilution factor of 6.3. The heating reduces the nucleation process and growth of volatile substances during the second dilution [32]. By multiplying the first dilution factor of the rotation disk diluter (16.5) by the second dilution (6.3), the total dilution factor is 104.

To determine the soot reactivity, a partial flow dilution tunnel (PFDT), Control Sistem 'Particulate Sampling System' PSS 20 from Control Sistem, which is shown in Fig. 6, is used [34]. The soot is sampled via a borehole probe, which is positioned approximately 0.3 m behind the EEPS. According to [35,36] and due to the short time span from the EEPS to the PSS 20, a change in particle morphology and chemical composition is negligible. The aerosol is then led by an ap proximately 0.5 m sample pipe to the PFDT in which it is diluted with filtered air and a dilution factor of 5 to prevent condensation. The temperature at the quartz fiber filters in the filter holder is set to 48 °C and controlled by heating the diluting air.

Before loading, the quartz fiber filters are conditioned for 24 h at 500 °C, so that volatile water and HC residues are reduced. Subsequently, the filters are loaded at the engine test bed. For the thermogravimetric analysis (TGA), the filters are preconditioned for 30 min at 150 °C. Then, a small amount of the filter is placed in a vessel on a high precision scale. TGA measurements are carried out from 50 °C to 849 °C employing a heating rate of 5 °C min^{-1}. A gas mixture of 95% N_2 and 5% O_2 is used. For evaluation, the temperature of the maximum weight loss rate T_{max} is usually used. Under the described conditions, the measurement uncertainty of T_{max} is 5 °C.

3.2. Engine setup

The used engine is a single cylinder research engine in a size typi cally employed in passenger cars. The main technical specifications are listed in Table 2.

The spark plug and the injector are placed in longitudinal direction to the camshafts between the inlet and outlet valves. A Bosch HDEV 5 injector with a six hole nozzle is used. The injector is mounted centrally in the cylinder.

A constant engine speed of 2000 min^{-1} is set for all experiments. In order to test the behavior with respect to thermodynamic parameters, gaseous emissions and particles of the alternative fuel, a start of in jection (SOI) variation with an indicated mean effective pressure (IMEP) of 0.5 MPa and 0.8 MPa is performed. The AF of 14.3 (air fuel equivalence ratio of 1) is the same for both fuels. An inlet temperature of 47 °C is set. The ignition angle is set to 22 °CAbTDCf and 16.5 °CAbTDCf for an IMEP of 0.5 MPa and 0.8 MPa, respectively. A variation of the SOI is performed between 330 °CAbTDCf and 230 °CAbTDCf. The rail pressure is set to 20 MPa. At the 0.5 MPa IMEP measuring point with an SOI at 330 °CAbTDCf, samples for the in vestigation of soot reactivity are taken.

In order to compare the knocking behavior of the fuels, the

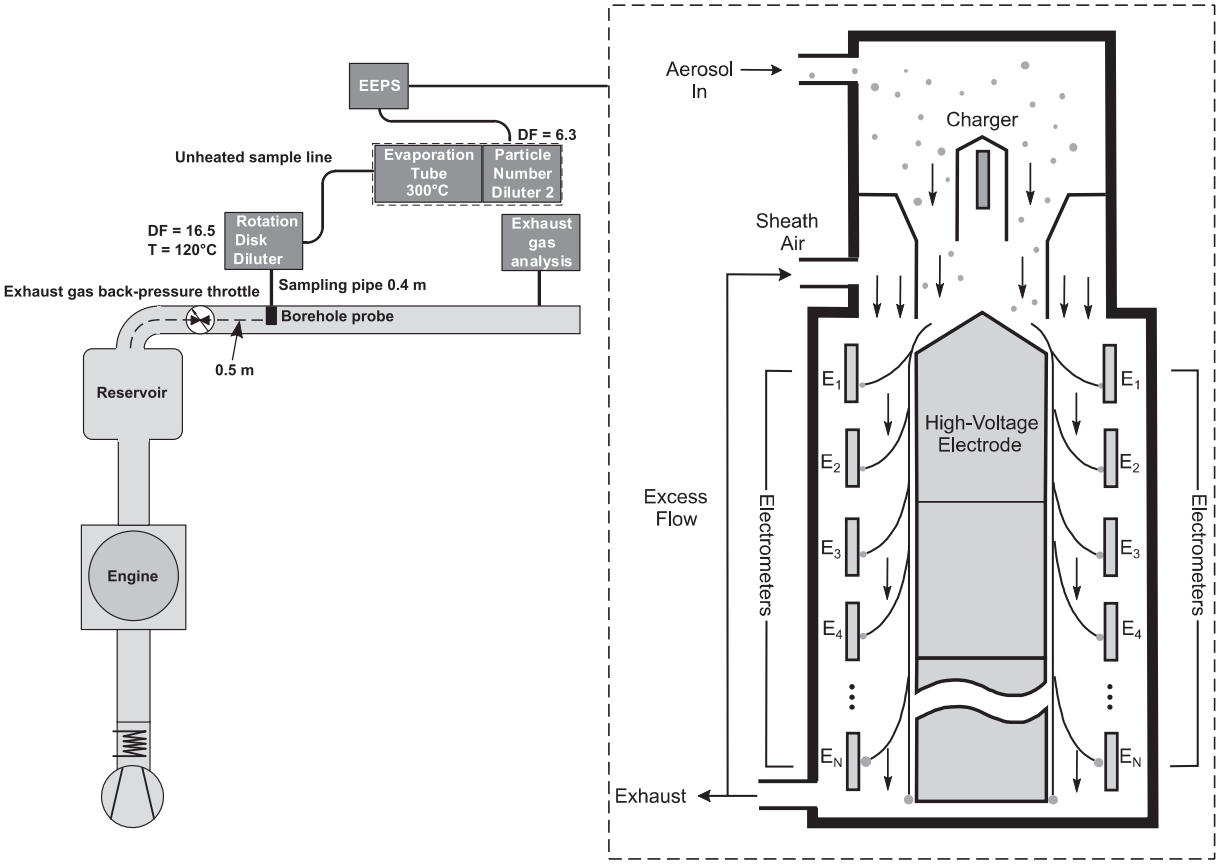

Fig. 5. Left: Schematic engine test bed setup for measuring PNC, TPNC, and HC (inspired by [33]). DF is the dilution factor and T the temperature. Right: Schematic structure of the TSI EEPS (Model 3090) [30].

Mannesmann VDO AG method [37] from the DEWETRON is used. The criterion for the knock limit is set to a value of 1.3 according to the above method. The experiments are performed at naturally aspirated full load conditions at an IMEP between 0.93 MPa and 0.94 MPa. To enhance knocking, the inlet temperature is increased to 80 °C. The SOI is set to 300 °CAbTDCf. The ignition angle is varied in 0.75 °CA steps in early direction until the knock limit criterion of 1.3 is reached.

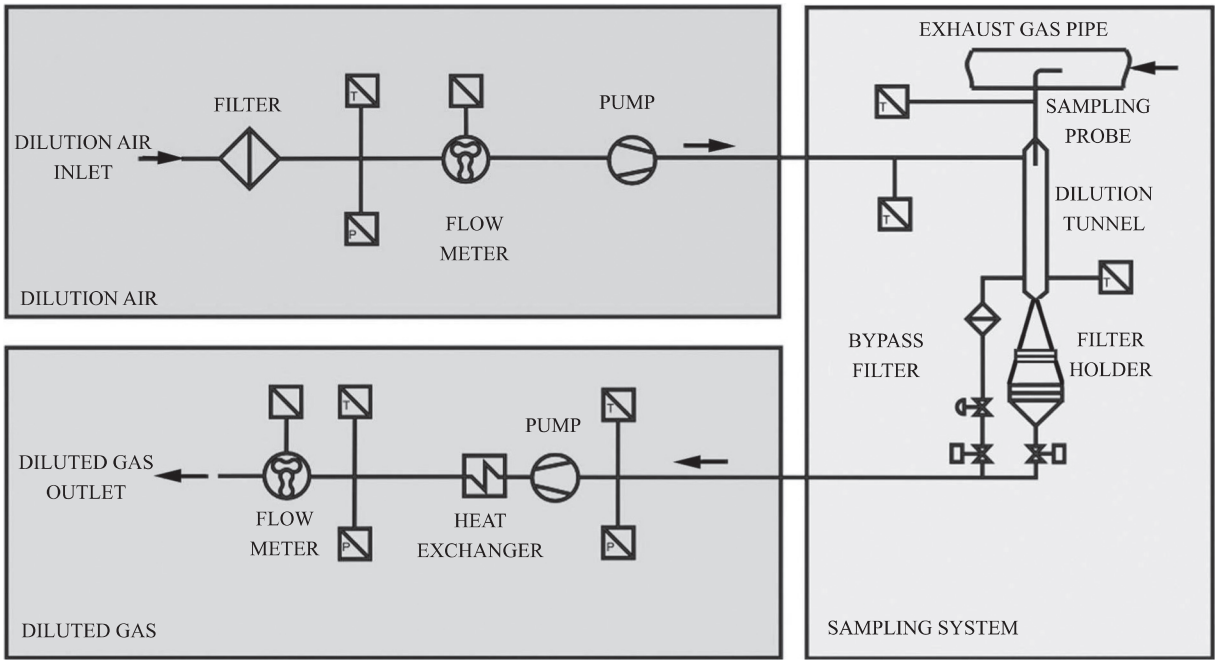

Fig. 6. Schematic setup of the PSS-20 partial flow dilution tunnel [34]. The quartz fiber filters are placed in the filter holder on the right (sampling system).

Table 2
Engine data.

Property	Value
Displaced volume/cc	498
Stroke/mm	90
Bore/mm	84
Compression ratio/–	10.5:1
Inlet valve spread/°CAbTDC	115
Outlet valve spread/°CAbTDC	100
Inlet/outlet valve lift/mm	8
Injection system	Centrally mounted DI
Rail pressure/MPa	20

4. Results and discussion

The study focuses on thermodynamics as well as exhaust gas com position. The former topic comprises knocking, flame development angle and rapid burn angle while the latter topic addresses particle and hydrocarbon emissions as well as soot reactivity.

4.1. Thermodynamics

For each in cylinder pressure of 200 consecutive cycles and the first law of thermodynamics, the heat release analysis according to Heywood [38] is performed. Regarding thermodynamic efficiency, an ideal center of combustion (COC) is crucial. It describes the crank angle value, at which 50% of the heat was released. This value can be ad justed by the ignition timing but is restricted by knocking. Thus, the knocking characteristics of the fuels are investigated in the beginning. The inflammation properties are described by the flame development angle (FDA). This angle is calculated by the difference between the start of combustion (at a cumulative heat release of 10%) and the ignition timing. Another significant contribution to thermodynamic efficiency is attributed to the rapid burn angle (RBA). This angle is the subtract between the angle at a cumulative heat release of 90% and the angle at the combustion start. The deviation from an infinitely fast combustion also reduces efficiency. This issue is considered below in the second part of the thermodynamics chapter. SI engines are subjected to high cyclic variations caused by various effects like in cylinder flow and mixture differences [39,40]. To determine the characteristic combus tion units explained above, an averaged cycle of 200 measured cycle is used. The variation of these units is gaussian distributed [41,42]. The combustion stability is described with the coefficient of variation of the IMEP (COV_{IMEP}), which is defined by the ratio of the standard deviation to the mean.

4.1.1. Knocking and efficiency

Fig. 7 shows the average of 200 in cylinder pressure cycles in the upper and the heat release rate in the lower graph. The in cylinder pressure of both fuels are shown with their envelopes (black and red shaded area). On the cumulative heat release curve, the COCs and their error bars, which indicate the standard deviation of the angle, are shown. Both curves are measured at the knock limit value of 1.3. The adjustment of the ignition angle at earlier spark timing is enabled by the higher research octane number of the bioliq®/10 fuel compared to the RON95 E5 fuel. An improvement of the ignition timing of 1.5 °CA, from 14.5 °CAbTDCf with the conventional RON95 E5 fuel to 16 °CAbTDCf with the bioliq®/10 fuel, can be observed. This results in an earlier and higher maximum of in cylinder pressure of 4.9 MPa at 18 °CAaTDCf in the case of bioliq®/10 compared to 4.5 MPa at 21 °CAaTDCf in the case of RON95 E5. Another effect is the improved center of combustion from 15.8 ± 2.1°CAaTDCf to 12.8 ± 1.8°CAaTDCf with the bioliq®/10. The IMEP increases from 0.93 MPa to 0.94 MPa. For both fuels a COV_{IMEP} of 0.01 was calculated. Therefore, the indicated power P_i can be calculated by Eq. (1)

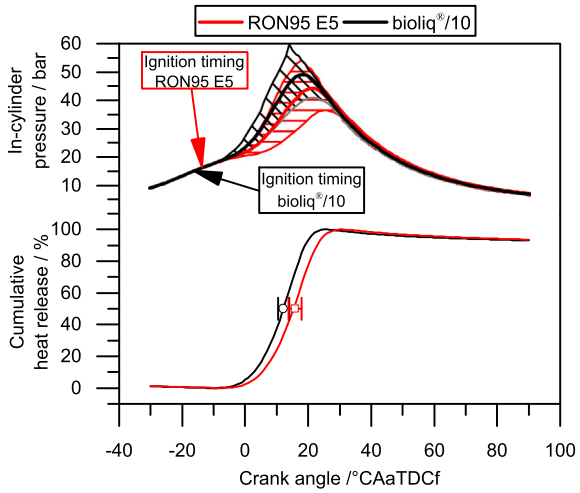

Fig. 7. In-cylinder pressure (upper graph) and integral of heat release rate (lower graph) at the knock limit at naturally aspirated full load and an inlet temperature of 80 °C of bioliq®/10 (black) and standard RON95 E5 (red). The upper graph shows the envelops of the two pressure curves. In the lower graph, both COC points with their standard deviation are additionally shown. (For interpretation of the references to colour in this figure legend, the reader is referred to the web version of this article.)

$$P_i = i * n * IMEP * V_H \tag{1}$$

The factor i indicates the number of ignitions per rotation. For a four stroke engine $i = 0.5$. The factor n is the engine speed and V_H is the displacement. The fuel mass flow of approximately 2.2 kg × h^{-1} is, due to the same lower heating value, identical for both fuels. This means, that the supplied heat is the same for both fuels. With the constant engine speed of 2000 min^{-1}, the constant displacement of 498 cc, and the same supplied heat, the differential indicated efficiency $\Delta\eta_i$ can be calculated by Eq. (2)

$$\Delta\eta_i = \frac{P_{i_{bioliq}}}{P_{i_{RON95E5}}} - 1 \tag{2}$$

As a result, the indicated efficiency increases about 1.1% in favor of bioliq®/10, based on reproducible measurements. The uncertainty of the differential indicated efficiency can be described by the COV_{IMEP} and uncertainties in the engine speed. With eq. (3), the difference in the indicated power can be calculated.

$$\Delta P_i = i * n * IMEP * COV_{IEMP} * V_H \tag{3}$$

To calculate the measurement uncertainty of the differntial in dicated efficiency, Eq. (3) can be integrated in Eq. (2). Due to the di vision of the two indicated powers, the relative error can be calculated by Eq. (4)

$$\frac{\Delta(\Delta\eta_i)}{\Delta\eta_i} = COV_{IMEP_{bioliq}} + COV_{IMEP_{RON95E5}} \tag{4}$$

With a COV_{IMEP} of 0.01 for both fuels, the relative uncertainty of the differential indicated efficiency is 2%. Therefore, the differential in dicated efficiency is calculated to 1.1% ± 0.022%.

The difference in engine speed was approx. 1 min^{-1}. At 2000 min^{-1}, the error is only 0.000005% and is therefore negligible.

By adding the bioliq® fuel to the RON95 E5, the ethanol content decreases by 0.3 Vol.−%. Due to the high octane number of 105 from ethanol [43], this would lead to a decrease in the bioliq®/10 blend's octane number. On the other hand, the decrease of the lower heating value by ethanol (26.9 MJ/kg [44]) is smaller in the bioliq®/10 blend due to the lower volumetric content of ethanol.

The bioliq®/10 blend has a higher content of aromatics. In parti cular toluene (RON: 124, LHV: 41.03 MJ/kg), m xylene (RON: 145,

LHV: 42.92 MJ/kg), o xylene (RON: 120, LHV: 41.25 MJ/kg) and 1,2,4 trimethylbenzene (RON: 109.5, LHV: 40) [45 47]. All aromatics have a higher RON than the ethanol. This fact in combination with the in creased content of these aromatics leads to an increase of the RON by 0.8 in the bioliq®/10 blend. Furthermore, most of these components have a smaller lower heating value than 42.39 MJ/kg. For this reason, there is a balance between the gain in lower heating value due to less ethanol, and the loss in lower heating value due to the aromatics.

Due to the identical lower heating values of the fuels, which means identical fuel consumption at same engine operation modes, and the improved ignition timing of bioliq®/10, which leads to an optimized COC, the thermal efficiency of bioliq®/10 is higher compared to RON95 E5. It has to be kept in mind, that this efficiency improvement is only relevant at high loads or in the case of knocking.

In summary, the higher aromatics content in the bioliq®/10 blend leads to an increase in RON of 0.8, which improves the knocking be havior. This was measured under full load lambda 1 condition. With bioliq®/10, the IMEP was increased by 0.01 MPa. Considering this in crease, and the COV_{IMEP}, an efficiency improvement of 1.1% ± 0.022% was calculated.

4.1.2. Characteristic combustion units

A rapid heat release rate calculation is used for the following comparison of the flame development angle, the center of combustion, the rapid burn angle and the combustion stability (COV_{IMEP}). The cal culation of each operation point is based on the mean value of 200 cy cles. The ignition timing is kept constant during the variation of the injection timing. The graphs in Fig. 8 show the results of the analysis for an IMEP of 0.8 MPa. Error bars are indicating the standard deviation of the combustion units. The standard deviations of the combustion units calculated from the pressure signals are in the range between 1 °CA and 3 °CA. This is due to the common variation of the combustion in SI engines. The mean value of these 200 cycles is reproducible. Therefore, it is possible to find trends, which are within the values of the standard deviation.

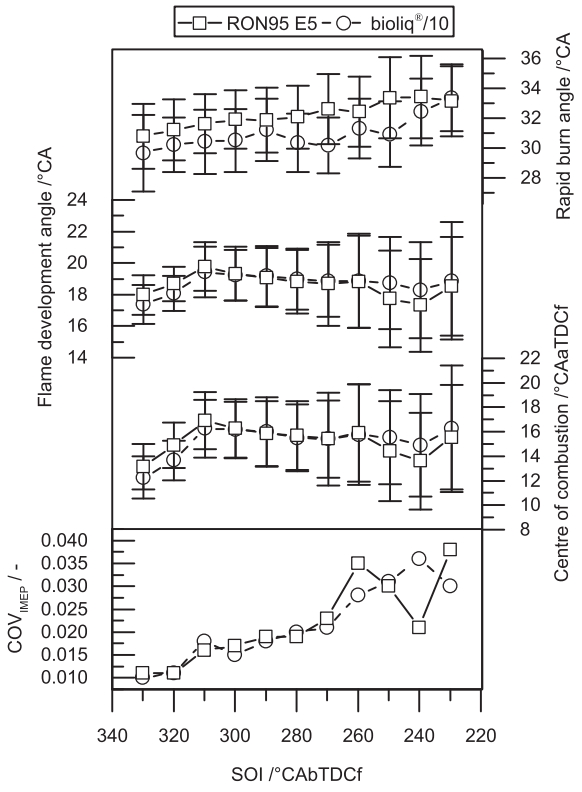

Fig. 8. Rapid burn angle (top), flame development angle (middle) and center of combustion (below) at 2000 min^{-1} with an engine load of 0.8 MPa and an ignition timing of 16.5 °CAbTDCf by a variation of SOI. The lowest graph shows the COV of the IMEP.

The flame development angle of both fuels is on the same level and varies from 16 to 22 °CA as a result of the SOI variation. At an earlier injection timing than 310 °CAbTDCf, bioliq®/10 shows an equal rapid burn angle as RON95 E5. An early start of injection reduces the flame development angle to the minimum of 17.5 °CA for the bioliq®/10. This reduction for both fuels can be explained by an interaction of the spray with the hot piston that helps to evaporate the fuel and a better mixture preparation, as an earlier SOI leaves more time for the mixing of air and fuel [48]. Due to the piston wetting, particle and HC emissions are also higher at these operating points.

The COC of the RON95 E5 is retarded from 13 to 17 °CAaTDCf for an SOI from 330 to 310 °CAbTDCf. In this area, bioliq®/10 shows a faster combustion with a 0.5 °CA earlier COC. Considering the standard deviation of the measurements, this reduction of COC is negligible. From 310 to 260 °CAbTDCf both fuels show the same COC at around 16 °CAaTDCf, considering the standard deviation, which is between 2.3 °CA and 4.1 °CA.

The rapid burn angle shows a difference for both fuels during the injection timing variation. bioliq® exhibits a constantly faster combus tion in its second half (50 to 90% heat release point). Fig. 8 shows a smaller average rapid burn angle of 1.2 °CA for a constant ignition timing and a constant COC between 310 and 260 °CAbTDCf. The cyclic variations are at their minimum with a COV of 1% of the indicated mean effective pressure at an SOI at 330 °CAbTDCf. A shift of the in jection to later timings decreases the combustion stability to 3.5% COV_{IMEP}. The exhaust valve is closed at 335 °CAbTDCf, which excludes fuel losses that might occur at an early SOI by scavenging unburned fuel into the exhaust system. For a later fuel injection than 260 °CAbTDCf, the cyclic variations of the IMEP are increasing up to 4%, due to the poor mixture preparation. This COV of 4% is comparable to the COVs of DISI engines in the literature [49]. The RON95 E5 shows a better be havior in these poor conditions with a 1 °CA earlier COC. The IMEP is decreasing almost linearly for later injection timings. At an SOI of 230 °CAbTDCf the remaining pressure is 95% of the maximum value. The losses can be explained by higher HC emissions (Fig. 14), increased combustion instability and a slower combustion.

The SOI variation at 0.5 MPa IMEP shows constant torque values for later fuel injections than 300 °CAbTDCf. The combustion stability and the emission of hydrocarbons are also stable for both fuels, contrary to the 0.8 MPa operation points. The IMEP is increasing for earlier in jection timings (330 °CAbTDCf). The tendency for the earlier end of combustion of bioliq®/10 at 0.8 MPa can be confirmed by the lower load points.

In summary, the heat release behavior of both fuels is nearly equal. The flame development angle and the center of combustion have si milar values with both tested fuels. Only at the second half of the combustion, the bioliq®/10 blend shows an approximately 1.2 °CA shorter rapid burn angle. Due to the same in cylinder flow conditions, the difference could be due to potentially different laminar burn velo cities, which have not yet been investigated. This influence has to be researched further.

4.2. Particles and HC concentration

In addition to the thermodynamic properties emissions have also been investigated in detail. In the following, particle emissions, soot reactivity and HC emissions are discussed.

4.2.1. Particles

The TPNC of standard RON95 E5 and bioliq®/10 during a variation of SOI at an IMEP of 0.5 MPa is shown in Fig. 9. The error bars represent the standard deviations from the averaged 1 Hz measurements. This deviation is for all measurement points in the range between $1 * 10^5$

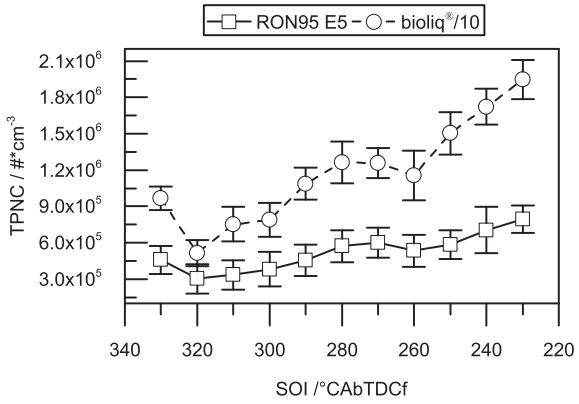

Fig. 9. Total particle number concentration as a function of SOI at an engine speed of 2000 min^{-1} and an IMEP of 0.5 MPa. The error bars show the standard deviation of the measurement.

$\#/cm^3$ to $2 * 10^5$ $\#/cm^3$ with both fuels. The wetting of the piston at the earliest SOI at 330 °CAbTDCf results in a local maximum of TPNC of $8.5 * 10^5$ $\#/cm^3$ and $4.0 * 10^5$ $\#/cm^3$ for the bioliq®/10 and the RON95 E5 respectively.

Both fuels show a global minimum at an SOI at 320 °CAbTDCf with TPNCs of $4.4 * 10^5$ $\#/cm^3$ and $2.6 * 10^5$ $\#/cm^3$, respectively. Afterwards, an increase in TPNC until an SOI of 280 °CAbTDCf to 260 °CAbTDCf is observed. The increase and the plateau afterwards are formed by liner and intake valve impingement like it is shown in [33,50,51]. The local maximum of TPNC is different with the maximum valve lift at 245 °CAbTDCf. This is due to the difference of the SOI electrical signal and the injection flow, and the penetration velocity of the spray. In addition [52] showed, that the liner impingement is probably due to unfavorable flow conditions.

Subsequently, the TPNC monotonously increases to its maximum of $1.45 * 10^6$ $\#/cm^3$ and $6.1 * 10^5$ $\#/cm^3$, respectively at the shortest mixed formation time at an SOI at 230 °CAbTDCf. According to [33], the engine has a low charge movement, which makes the time for mixture formation more important.

It is noticeable that bioliq®/10 produces remarkably more particles compared to RON95 E5. Several studies revealed a correlation between the distillation curve in combination with aromatics and the particle emission [53,54]. This combination is the most likely effect of the stronger increase in TPNC of bioliq®/10 at later SOIs compared to RON95 E5. The higher evaporation temperature in the range of 30% 80% of the distillation curve and the aromatics $\geq C_9$ of bioliq®/10 leads also to the increased and faster particle growing.

In Fig. 10 a PSD comparison of the two fuels, at two different SOI's, at an engine load of 0.5 MPa is shown with a logarithmic x axis. Each marker indicates one size class of the EEPS. In this figure, the error bars indicate the standard deviation of the measurements. Especially for particles smaller than 20 nm the deviation is high. This can be explained by the relatively small number of these particles, which is close to the detection limit (red line) of EEPS in this diameter range. The upper graph shows the PSD at 330 °CAbTDCf and the lower graph at 320 °CAbTDCf. At the earlier SOI, the bioliq®/10 shows a higher PNC of $6.3 * 10^4$ $\#/cm^3$ in its accumulation mode (electrical mobility diameter > 23 nm) at the 52.3 nm class. In comparison to this, the RON95 E5 shows a lower PNC of $2.6 * 10^4$ $\#/cm^3$ at a smaller particle size class of 39.2 nm. With the later SOI at 320 °CAbTDCf the particle size class of maximum PNC of the bioliq®/10 remains the same, but the PNC is reduced to $2.8 * 10^4$ $\#/cm^3$.

Especially the high peak at the 10.8 nm class with a PNC of $4.4 * 10^4$ $\#/cm^3$ is noticeable for an increase in nucleation mode (electrical mobility diameter < 23 nm). Considering the standard deviation for particles below 23 nm, no difference between the two fuels can be found. Only the accumulation mode particle class of the RON95 E5

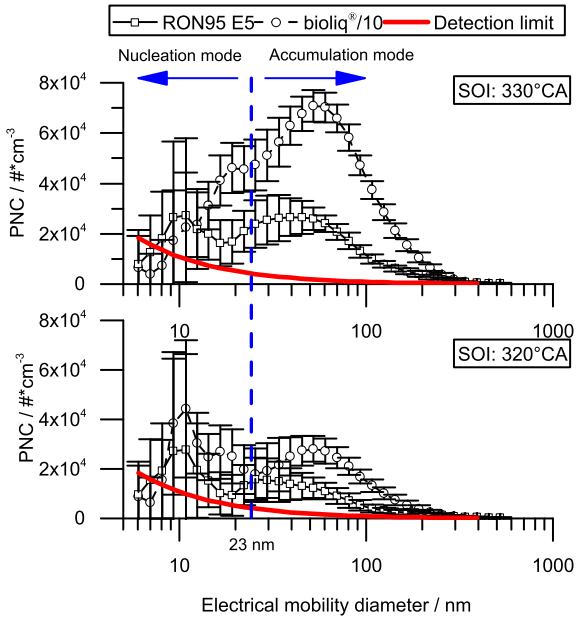

Fig. 10. Particle size distribution at an engine speed of 2000 min^{-1} and an IMEP of 0.5 MPa. The upper graph shows the PSD at an SOI at 330 °CAbTDCf. The lower graph shows the PSD at an SOI at 320 °CAbTDCf. Additionally, the detection limit of the EEPS is displayed (red line). The error bars show the standard deviation of the measurement. The vertical blue dotted line indicates the separation of the nucleation and accumulation mode. (For interpretation of the references to colour in this figure legend, the reader is referred to the web version of this article.)

decreases to a diameter of 25.5 nm with a lower PNC of $1.6 * 10^4$ $\#/cm^3$. According to [55], the PSD tends to have larger particles under pool fire conditions. By changing the SOI from 330 °CAbTDCf to 320 °CAbTDCf, the pool fire is reduced. Therefore, the PNC in the larger accumulation mode decreases. References [56,57] show, that higher aromatics promote the formation of polycyclic aromatic hydrocarbons (PAH) during combustion. These PAHs are precursors for soot formation. As mentioned before, the higher content of C 9, and larger, aromatics of bioliq®/10 leads to an increased and faster particle growing. Thus, the PNC and electrical mobility diameter at PNC peak of the accumulation mode increases. In addition to this, the evaporation curve is slightly higher for the bioliq®/10.

In summary, it is possible that the higher aromatics content in the fuel and the higher evaporation temperatures in the 30% to 80% range result in an increase of TPNC and PNC in nucleation and accumulation mode [58].

The TPNC as a function of SOI at an IMEP of 0.8 MPa is shown in

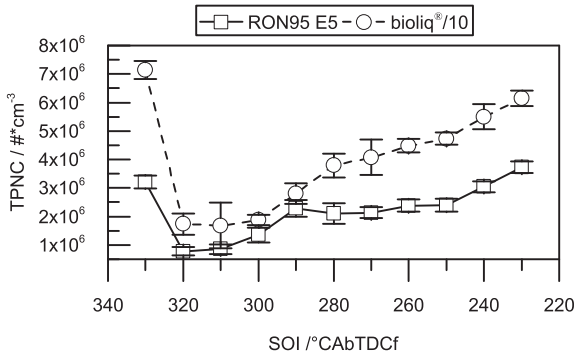

Fig. 11. Total particle number concentration as a function of SOI at an engine speed of 2000 min^{-1} and an IMEP of 0.8 MPa. The error bars show the standard deviation of the measurement.

Fig. 11. The TPNC reaches its global maximum at the earliest 330 °CAbTDCf SOI in the case of both fuels. These high TPNCs are caused by piston impingement. As in the case of measurements with an IMEP of 0.5 MPa, the TPNC of bioliq®/10 ($7.8 * 10^6$ #/cm^3) is higher than the TPNC of RON95 E5 ($3.3 * 10^6$ #/cm^3). This higher TPNC of bioliq®/10 results from the higher content of heavier aromatics. These heavier aromatics have an increased evaporation temperature. There fore, the diffusion flame, which leads to increased particle forming, is more pronounced.

With respect to the measurement uncertainty, a saddle point, which forms the global minimum, between an SOI at 320 and 310 °CAbTDCf (RON95 E5) and until 290 °CAbTDCf (bioliq®/10) can be observed. Thereafter, a monotonous increase in TPNC with later injection is ob served for bioliq®/10. This trend is different from the plateau of RON95 E5. In the range between an SOI of 300 °CAbTDCf to 250 °CAbTDCf the effect of liner and intake valve spray interaction is the main reason for both trends. The higher evaporation temperature in case of bioliq®/10 leads to a more pronounced diffusion flame.

After an SOI of 250 °CAbTDCf, the time for mixture formation is too short. Therefore, inhomogeneities in the charge causes the increasing TPNC. In all measurements the standard deviation is in the range of $1.4 * 10^5$ #/cm^3 to $3.7 * 10^5$ #/cm^3 with RON95 E5 and $1.8 * 10^5$ #/cm^3 to $8.0 * 10^5$ #/cm^3 with the bioliq®/10 blend.

The basic behavior of PSD at the 0.8 MPa measuring point (Fig. 12) is similar to that at the lower engine load of 0.5 MPa (Fig. 10). Also in this figure the x axis is logarithmic, the error bars show the standard deviation of the measurement, the red line is the detection limit of the EEPS and the vertical blue dotted line is the 23 nm separation between nucleation and accumulation mode.

At the early SOI at 330 °CAbTDCf (upper graph) bioliq®/10 exhibits a maximum of the PNC at the 80.6 nm particle diameter class while RON95 E5 exhibits a maximum at the 69.8 nm class. The size classes are next to each other. Therefore, it is difficult to differentiate between the

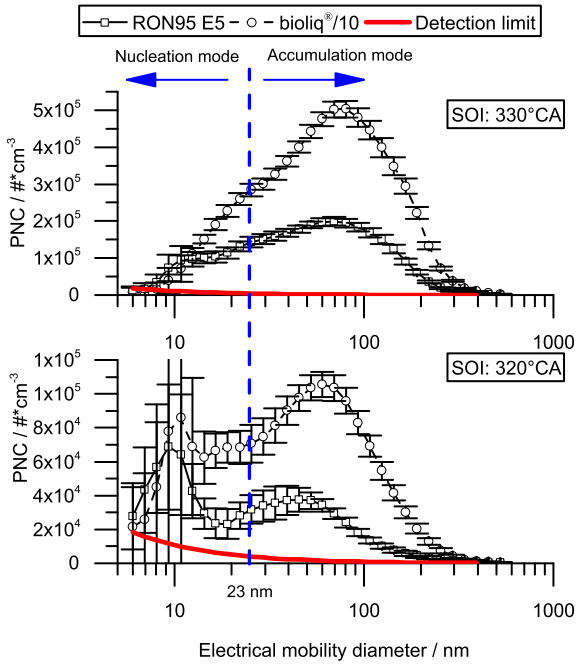

Fig. 12. Particle size distribution at an engine speed of 2000 min^{-1} and an IMEP of 0.8 MPa. The upper graph shows the PSD at an SOI at 330 °CAbTDCf. The lower graph shows the PSD at an SOI at 320 °CAbTDCf. Additionally, the detection limit of the EEPS is displayed (red line). The error bars show the standard deviation of the measurement. The vertical blue dotted line indicates the separation of the nucleation and accumulation mode. (For interpretation of the references to colour in this figure legend, the reader is referred to the web version of this article.)

two particle sizes. This is due to the possibility of the real particle size of approx. 75 nm. These particles can be measured in both classes. Thus no influence of the particle electrical mobility diameter of the fuel can be measured.

However, the PNC peak in the accumulation mode of bioliq®/10 is 2.5 times higher than the PNC of RON95 E5, which is at $2.0 * 10^5$ #/cm^3. Because of the high PNC, the measurements have a high re produciblity and a relatively small standard deviation. By changing the SOI by 10 °CA towards late, the particle diameters in the accumulation mode decrease to 60.4 nm for bioliq®/10 and 45.3 nm for RON95 E5. Furthermore, a decrease of PNC at peak to $1.1 * 10^5$ #/cm^3 (bioliq®/10) and $3.8 * 10^4$ #/cm^3 (RON95 E5) can be observed.

An increase of the small 10.8 nm class is also observed. However, considering the standard deviation at small particles in the range of 10 nm, no difference between RON95 E5 and bioliq®/10 at these electrical mobility diameters can be measured. The change in electrical mobility diameter at PNC peak and the lower PNC peak can be ex plained by the reduction of pool fire again. Due to the distillation curve characteristic of bioliq®/10, the effect of pool fire should be more dominant compared to RON95 E5. Therefore, at the 320 °CAbTDCf a higher PNC at the larger accumulation mode is measured.

In summary, bioliq®/10 shows an increased particle formation at the investigated engine loads. Its behavior at different SOIs differ entiates only slightly from the standard RON95 E5 fuel. The higher particle emissions may be due to the higher aromatics content, espe cially of the C_{9+} aromatics [59,60], and the slightly higher evaporation curve of bioliq®/10 [61,62]. By optimizing the SOI, the TPNC can be reduced as shown in Figs. 9 and 11 for the bioliq®/10 fuel. However, even at its best point and, when considering the TPNC, and by con sidering the standard deviation, the bioliq®/10 blend produces twice as much particles.

The PSD difference of both fuels is more critical with regard to GPFs. Their filtration efficiency depends strongly on the PSD of the aerosol, which enters into the system. In the case of small particle diameters until approximately 20 nm, this efficiency is very high. Several studies reveal a reduction of filtration efficiency in the range of 20 nm to 400 nm [63 65]. The bioliq®/10 PSD has its diameter at peak values (52.3 nm to 80.6 nm) in this range. The bioliq®/10 exhibits diameters in this range, which are more counterproductive to the filtration efficiency of current GPFs than the PSD of the conventional RON95 E5.

4.2.2. Reactivity of soot

The regeneration properties of GPFs as well as diesel particulate filters are strongly influenced by the reactivity of soot [66]. As an in dicator for the reactivity of soot the shape of the derivate mass reduc tion over the temperature and especially the temperature at the max imum gradient of mass reduction (T_{max}) is used [67].

This derivate mass reduction over temperature function is shown in Fig. 13 at the 0.5 MPa measuring point and an SOI at 330 °CAbTDCf. Both fuels show a global maximum at a temperature of about 170 °C. At this temperature no reaction of soot is expected according to different publications [67,68]. Furthermore, a post connected FTIR did not show a release of CO_2 or CO. It is therefore likely, that this peak is due to the release of PAHs or volatile particles.

At a temperature of 340 °C, for both soots a shoulder emerges. Regarding RON95 E5, this shoulder is significantly broader compared to bioliq®/10. The shape of the curves between 300 °C and 660 °C is very different and the curve of RON95 E5 shows a more bi modal characteristic than the curve of bioliq®/10. Considering the PSD at this operation point, there seems to be two kinds of soot for RON95 E5, one with very small particles and one with larger particles. This results in a wider shape of the curve in the specified temperature range due to superimposition of two peaks [69,70]. According to [71 73], the higher surface volume ratio of smaller particles results in an oxidation at lower temperatures. Therefore, the shoulder in the case of RON95 E5 is most probably caused by the small 10 nm particles. Similarly, the small

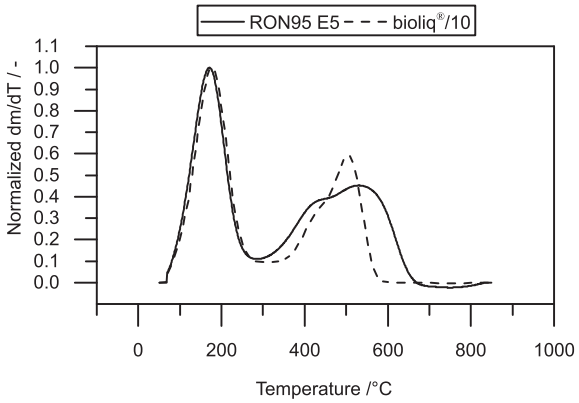

Fig. 13. TGA of soot residues obtained at an engine speed of 2000 min^{-1}, an IMEP of 0.5 MPa and an SOI at 330 ˚CAbTDCf.

shoulder at 450 ˚C in the case of bioliq®/10 can be assigned to the small particles with a diameter around 19.1 nm. With respect to the ratio of the maximum PNC, this peak is less significant compared to the cor responding peak of RON95 E5. It is therefore less pronounced.

The T_{max} for both fuels are different, also considering the mea surement uncertainty of ± 5 ˚C. In the case of bioliq®/10 T_{max} is 506 ˚C and thus, soot reactivity is higher than in the case of RON95 E5, with a T_{max} of 530 ˚C. Accordingly, the larger particles in the case of bioliq®/ 10 exhibit a better reactivity, which is in contrast to the better surface volume ratio of the smaller particles of RON95 E5. A reason for this behavior could be a different particle morphology. Another possible explanation is the difference in the initial fuel identity as described by [74]. Additionally, ref. [75] mentioned a dependence of the soot re activity on the aromatics content.

In summary, soot reactivity in the case of bioliq®/10 is, despite of the larger peak diameter, slightly higher than in the case of RON95 E5 which is beneficial for the regeneration of particulate filter systems in the exhaust gas after treatment. Especially the bi and nearly mono modal trends of PSDs, of RON95 E5 and bioliq®/10, are visible in the results of the TGA (shown in Fig. 10). The mono modal trend of bioliq®/ 10 indicates the formation of particles of a preferred species. Therefore, a sharp peak with only a slightly pronounced shoulder is visible. On the other hand, the bi modal trend of RON95 E5 points to several particle types. These manifests themselves in a significantly broader distribution of the oxidation process. The temperature range of the reactivity is in good agreement with [76].

4.2.3. Hydrocarbons

Hydrocarbons (HC) are considered to be particularly harmful. To investigate HC emissions, engine runs at an engine speed of 2000 min^{-1} and an IMEP of 0.5 MPa and 0.8 MPa have been carried out.

In Fig. 14 HC concentrations at the 0.5 MPa measuring point as a function of SOI are shown. The error bars are indicating the measure ment inaccuracy of the FID. This measurement inaccuracy depends on the measured HC concentration. It is in the range between 16 ppm and 27 ppm for both fuels.

As for particle emissions, bioliq®/10 shows a higher HC con centration than RON95 E5. The maximum concentration is for both fuels at the earliest SOI at 330 ˚CAbTDCf. At this operation point, the HC concentration of bioliq®/10 is 880 ppm, about 200 ppm higher compared to RON95 E5. The reason is the strong piston impingement in combination with the more favorable distillation curve of RON95 E5.

After that, the HC concentration decreases until an SOI of 300 ˚CAbTDCf. Considering the measurement uncertainty of approxi mately 18 ppm, the lowest HC concentrations are at an SOI of 300 ˚CAbTDCf and 250 ˚CAbTDCf. The later SOI reduces the piston impingement, which is more favorable for the HC emissions as well. The HC concentration of RON95 E5 is 574 ppm ± 17 ppm. With the

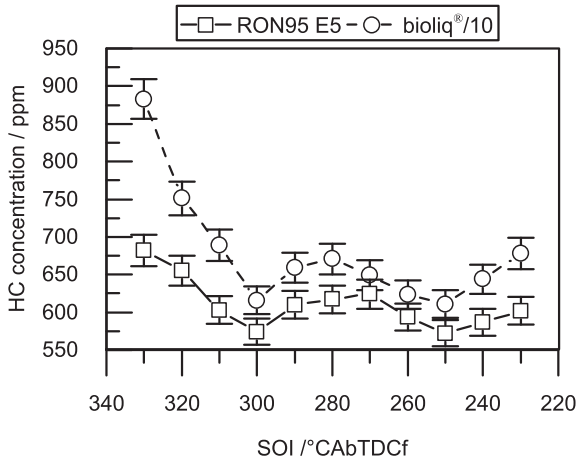

Fig. 14. HC concentration at an engine speed of 2000 min^{-1}, an IMEP of 0.5 MPa and a rail pressure of 20 MPa. The error bars indicate the measurement inaccuracy of the FID used.

bioliq®/10 blend, this concentration is only slightly higher (616 ppm ± 19 ppm). This difference may be due to the more fa vorable distillation curve of RON95 E5 and the higher aromatics con tent of bioliq®/10 [77,78].

Between 300 ˚CAbTDCf and 270 ˚CAbTDCf the liner impingement results in an increasing HC emission [50]. Due to the maximum lift of the intake valve at 245 ˚CAbTDCf and the difference between SOI signal and the injection flow, and the propagation velocity of the spray, there is a possibility of a combination on liner and intake valve impingement, described above. This leads to an increase in HC emissions to its max imum at 280 ˚CAbTDCf and 270 ˚CAbTDCf with bioliq®/10 blend and RON95 E5. The higher HC emission of the bioliq®/blend is thus due to its distillation curve and the aromatics. The second minimum is created due to the less significant intake valve spray interaction. Afterwards, the HC emission increases due to the shortened mixture formation.

The HC concentration at nearly full engine load, i.e. at an ambient air aspirated engine mode with an IMEP of 0.8 MPa, is shown in Fig. 15. Due to the lower HC emissions, the measurement inaccuracy is with 16 ppm to 25 ppm smaller. As in the case of an IMEP of 0.5 MPa (Fig. 14), the fuels perform similarly in case of the higher HC con centration with bioliq®/10.

For an SOI at 330 ˚CAbTDCf, local maxima of HC concentration of 710 ppm and 580 ppm are observed with bioliq®/10 and RON95 E5,

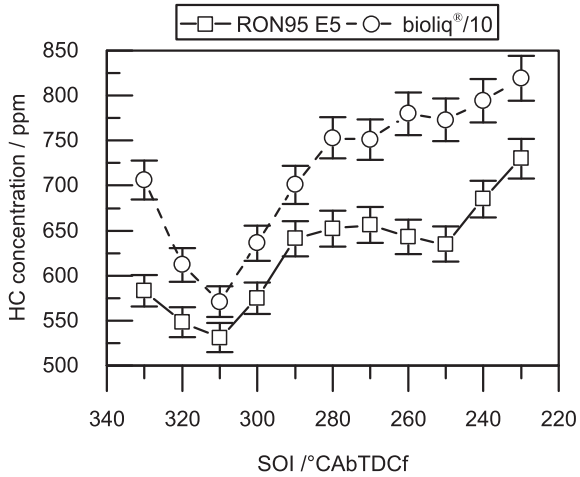

Fig. 15. HC concentration at an engine speed of 2000 min^{-1}, an IMEP of 0.8 MPa and a rail pressure of 20 MPa. The error bars indicate the measurement inaccuracy of the FID used.

respectively. This is also due to the effect of piston impingement. In comparison to the 0.5 MPa load, the HC concentration is approx. between 150 ppm and 200 ppm lower. This is due to the higher in cylinder pressure, which reduces the propagation velocity of the spray, and the hotter piston [50], which increases the fuel evaporation. Here again, the distillation curve of the fuel is the most probable reason for the difference between RON95 E5 and bioliq®/10. The HC concentration of both fuels decreases until an SOI at 310 °CAbTDCf.

After that, the HC concentration increases, due to the liner impingement, until an SOI of 270 °CAbTDCf (RON95 E5) and 280 °CAbTDCf (bioliq®/10), respectively. Thereafter, the curves of both fuels exhibit a plateau until an SOI of 250 °CAbTDCf. Like before at the 0.5 MPa load point, this plateau is probably created by the liner and intake valve spray interaction. This interaction is reduced with later SOI's, which leads to this plateau. In this area the difference between the bioliq®/10 and RON95 E5 is especially large. This difference might be caused by an higher impingement of the liner and the intake valve. One reason is again the distillation behavior according to distillation curve, which leads to a higher spray penetration.

In comparison to the overall trend of this increase and plateau in HC emission with the 0.5 MPa engine load, the second minimum is missing. One of the most probable reasons is the absence of the 'flash boiling effect' [79,80]. At the lower engine load the in cylinder pressure at SOI is in the range of 50 kPa, which is lower than the vapor pressure of both fuels. The in cylinder pressure at the 0.8 MPa load is with 90 kPa higher and above the vapor pressure of both fuels. Therefore, this effect is not expected at this engine load. However, further studies on spray formation still need to be done to investigate these effects in more detail. By shifting the SOI to later timings the HC concentration increases slightly. The different distillation curves could be a promising starting point for further investigations and development of the fuel [56].

As stated above, the HC concentration in the case of bioliq®/10 is under all conditions higher than in the case of RON95 E5. According to the literature, this cannot be explained by an increased aromatics content of bioliq®/10. The main reason for higher HC emissions is probably the distillation curve of bioliq®/10 at somewhat higher temperatures. This theory is encouraged by a stronger dependency of the emissions by spray component interactions. However, with an optimized SOI it is possible to achieve HC concentrations for the bioliq® fuel, which are similar to those of RON95 E5.

5. Conclusion

The bioliq® process comprises the entire process chain from renewable feedstocks to the production of hydrocarbons. The core technologies are fast pyrolysis of biomass, gasification of the resulting pyrolysate, cleaning of the obtained synthesis gas, conversion to DME and, finally, DME conversion to gasoline type hydrocarbons. The liquid product is fractionated by rectification resulting in a mixture with an aromatics content of about 75 wt.−%.

The mixture has been blended with conventional RON95 E5 gasoline and a content of 10 Vol.−% of bioliq® gasoline has been adjusted. The blend (bioliq®/10) meets the DIN EN 228 standard for automotive fuels and its combustion properties have been investigated in terms of efficiency and emissions. A comparison of bioliq®/10 with neat RON95 E5 revealed an improved knocking behavior of bioliq®/10 and thus, a higher efficiency. Particle as well as hydrocarbon emissions in the case of bioliq®/10 are significantly higher than for RON95 E5. Increased particle emissions are attributed to the higher content of aromatics. Particle and hydrocarbon emissions can be reduced by control of the engine parameters, especially by optimizing the SOI. Regarding soot reactivity, soot from bioliq®/10 exhibits higher reactivity than that from RON95 E5.

Current work concentrates on the fuel production with a reduced content of aromatics, e.g. by tuning rectification and/or chemical upgrading. Regarding the latter strategy, several procedures are considered such as hydrogenation, hydrodealkylation, isomerization or combinations thereof. These procedures must be technically adapted to the products of the bioliq® process, considering the investment and operating costs of a later process. Another option is an improved fuel production with a high selectivity for the desired components. To realize this, not only highly optimized reaction conditions are needed but also highly efficient catalysts which lead directly to well suited fuels. Major objective is the direct synthesis of an optimized fuel which meets the current standards and allows for high CO_2 savings either by high blending ratios or, ideally, by use of the pure fuel.

Abbreviations

AF	Air fuel ratio
CAaTDCf	Crank angle after top dead center firing
CAbTDCf	Crank angle before top dead center firing
COC	Center of combustion
COV	Coefficient of variation
DI	Direct injection
DME	Dimethyl ether
DTG	DME to gasoline
DVPE	Dry vapor pressure equivalent
EEPS	Engine exhaust particle sizer
FID	Flame ionization detector
FTIR	Fourier transform infrared spectrometer
GPF	Gasoline particulate filter
HC	Hydrocarbon
IMEP	Indicated mean effective pressure
LHV	Lower heating value
MON	Motor octane number
PAH	Polycyclic aromatic hydrocarbons
PFDT	Partial flow dilution tunnel
PM	Particulate matter
PN	Particle number
PNC	Particle number concentration
PSD	Particle size distribution
PSS	Particulate Sampling System
RON	Research octane number
SOI	Start of injection
T_{max}	Temperature at maximum peak
TGA	Thermogravimetric analysis
TPNC	Total particle number concentration

Declaration of competing interest

The authors declare that they have no known competing financial interests or personal relationships that could have appeared to influence the work reported in this paper.

Acknowledgements

Financial support from the 'Ministerium für Wissenschaft, Forschung und Kunst Baden Württemberg' (project 'Profilregion Mobilitätssysteme Karlsruhe', project no. AZ.:32 7544 0/76/6), the 'Helmholtz Research School Energy Related Catalysis' and the 'Strategiedialog Automobilwirtschaft in the project reFuels Kraftstoffe neu denken' is gratefully acknowledged. The authors are grateful to the 'Bundesministerium für Ernährung und Landwirtschaft (BMEL)' and 'Fachagentur Nachwachsende Rohstoffe e.V. (FNR)', the 'Helmholtz Gemeinschaft Deutscher Forschungszentren (HGF)', the 'Ministerium für Wirtschaft, Arbeit und Wohnungsbau Baden Württemberg' and the 'Ministerium für Wissenschaft, Forschung und Kunst Baden Württemberg' for financing the bioliq® plant. The authors also thank Doreen Neumann Walter, Herbert Lam and Gerd Ullrich for technical support.

References

[1] Klimaschutzplan 2050: Klimaschutzpolitische Grundsätze und Ziele der Bundesregierung, URL, 2019. https://www.bmu.de/fileadmin/Daten BMU/Download PDF/Klimaschutz/klimaschutzplan 2050 bf.pdf.

[2] European Commission, A clean planet for all: a European strategic long-term vision for a prosperous, modern, competitive and climate neutral economy, https://eur-lex.europa.eu/legal-content/EN/TXT/?uri=CELEX:52018DC0773, (2018).

[3] K. Donaldson, V. Stone, A. Clouter, L. Renwick, W. MacNee, Ultrafine particles, Occupational and Environmental Medicine 58 (3) (2001) 211–216 199 https://doi.org/10.1136/oem.58.3.211.

[4] J. Heyder, P. Brand, J. Heinrich, A. Peters, G. Scheuh, T. Tuch, E. Wichmann, Size distribution of ambient particles and its relevance to human health, 2nd Colloquium on Particulate Air Pollution and Health, Park City, Utah, Vol. 1 1996.

[5] V. Stone, M.R. Miller, M.J.D. Clift, A. Elder, N.L. Mills, P. Møller, R.P.F. Schins, U. Vogel, W.G. Kreyling, K. Alstrup Jensen, T.A.J. Kuhlbusch, P.E. Schwarze, P. Hoet, A. Pietroiusti, A. de Vizcaya-Ruiz, A. Baeza-Squiban, J.P. Teixeira, C.L. Tran, F.R. Cassee, Nanomaterials Versus Ambient Ultrafine Particles: an Opportunity to Exchange Toxicology Knowledge, Environ. Health Perspect. 125 (10) (2017) 106002, https://doi.org/10.1289/EHP424.

[6] A. Mamakos, U. Manfredi, Physical Characterization of Exhaust Particle Emissions From Late Technology Gasoline Vehicles, Vol. 25382 Publications Office, Luxembourg, 2012 of EUR (Luxembourg).

[7] T. Boger, N. Gunasekaran, R. Bhargava, C. Bischof, Partikelfiltertechniken für DI-Ottomotoren, MTZ - Motortechnische Zeitschrift 74 (6) (2013) 452–458, https://doi.org/10.1007/s35146-013-0127-1.

[8] R.-U. Dietrich, F.G. Albrecht, S. Maier, D.H. König, S. Estelmann, S. Adelung, Z. Bealu, A. Seitz, Cost calculations for three different approaches of biofuel production using biomass, electricity and CO2, Biomass Bioenergy 111 (2018) 165–173.

[9] E. Dinjus, U. Arnold, N. Dahmen, R. Höfer, W. Wach, Green fuels–sustainable solutions for transportation, Sustainable Solutions for Modern Economies, vol. 4, 2009, p. 125.

[10] R. Ahmad, M. Hellinger, M. Buchholz, H. Sezen, L. Gharnati, C. Wöll, J. Sauer, M. Döring, J.-D. Grunwaldt, U. Arnold, F lame-made Cu/ZnO/Al2O3 catalyst for dimethyl ether production, Catalysis Communications 43 (2014) 52–56, https://doi.org/10.1016/j.catcom.2013.08.020 http://www.sciencedirect.com/science/article/pii/S1566736713003294.

[11] U. Arnold, P. Haltenort, K. Herrera Delgado, B. Niethammer, J. Sauer, Die Rolle von Dimethylether (DME) als Schlüsselbaustein synthetischer Kraftstoffe aus erneuerbaren Rohstoffen, in: W. Maus (Ed.), Zukünftige Kraftstoffe, Vol. 92 of ATZ/MTZ-Fachbuch, Springer, Berlin, Berlin, 2019, pp. 532–561, , https://doi.org/10.1007/978-3-662-58006-6 22.

[12] E. Dinjus, N. Dahmen, Das Bioliq-Verfahren Konzept, Technologie Und Stand Der Entwicklung, MTZ - Motortechnische Zeitschrift 71 (12) (2010) 864–868, https://doi.org/10.1007/BF03225630.

[13] N. Dahmen, E. Dinjus, T. Kolb, U. Arnold, H. Leibold, R. Stahl, State of the art of the bioliq process for synthetic biofuels production, Environ. Prog. Sustain. Energy 31 (2) (2012) 176–181, https://doi.org/10.1002/ep.10624.

[14] N. Dahmen, J. Abeln, M. Eberhard, T. Kolb, H. Leibold, J. Sauer, D. Stapf, B. Zimmerlin, The bioliq process for producing synthetic transportation fuels, Wiley Interdisciplinary Reviews: Energy and Environment 6 (3) (2017) e236, , https://doi.org/10.1002/wene.236.

[15] F. Trippe, M. Fröhling, F. Schultmann, R. Stahl, E. Henrich, Techno-economic analysis of fast pyrolysis as a process step within biomass-to-liquid fuel production, Waste and Biomass Valorization 1 (4) (2010) 415–430, https://doi.org/10.1007/s12649-010-9039-1.

[16] N. Dahmen, E. Henrich, E. Dinjus, F. Weirich, The bioliq bioslurry gasification process for the production of biosynfuels, organic chemicals, and energy, energy, Sustainability and Society 2 (1) (2012) 3, https://doi.org/10.1186/2192-0567-2-3.

[17] C. Pfitzer, N. Dahmen, N. Tröger, F. Weirich, J. Sauer, A. Günther, M. Müller-Hagedorn, Fast Pyrolysis of Wheat Straw in the Bioliq pilot Plant, Energy Fuel 30 (10) (2016) 8047–8054, https://doi.org/10.1021/acs.energyfuels.6b01412.

[18] T. Kolb, M. Aigner, R. Kneer, M. Müller, R. Weber, N. Djordjevic, Tackling the challenges in modelling entrained-flow gasification of low-grade feedstock, J. Energy Inst. 89 (4) (2016) 485–503, https://doi.org/10.1016/j.joei.2015.07.007.

[19] S. Seebold, M. Eberhard, G. Wu, E. Yazhenskikh, D. Sergeev, T. Kolb, M. Müller, Thermophysical and chemical properties of bioliq slags, Fuel 197 (2017) 596–604, https://doi.org/10.1016/j.fuel.2017.02.027.

[20] M. Eberhard, U. Santo, D. Böning, H. Schmid, B. Michelfelder, B. Zimmerlin, A. Günther, P. Weigand, M. Müller-Hagedorn, D. Stapf, T. Kolb, Der bioliq-Flugstromvergaser - ein Baustein der Energiewende, Chemie Ingenieur Technik 90 (1–2) (2018) 85–98, https://doi.org/10.1002/cite.201700086.

[21] M. Stiefel, R. Ahmad, U. Arnold, M. Döring, Direct synthesis of dimethyl ether from carbon-monoxide-rich synthesis gas: influence of dehydration catalysts and operating conditions, Fuel Process. Technol. 92 (8) (2011) 1466–1474, https://doi.org/10.1016/j.fuproc.2011.03.007.

[22] R. Ahmad, D. Schrempp, S. Behrens, J. Sauer, M. Döring, U. Arnold, Zeolite-based bifunctional catalysts for the single step synthesis of dimethyl ether from CO-rich synthesis gas, Fuel Process. Technol. 121 (2014) 38–46, https://doi.org/10.1016/j.fuproc.2014.01.006.

[23] R. Ahmad, U. Arnold, D. Deutsch, M. Döring, J. Sauer, Passivation and reactivation of catalyst systems for the single step synthesis of dimethyl ether from CO-rich synthesis gas, J. Mol. Catal. A Chem. 422 (2016) 207–215, https://doi.org/10.1016/j.molcata.2015.12.029.

[24] B. Niethammer, S. Wodarz, M. Betz, P. Haltenort, D. Oestreich, K. Hackbarth, U. Arnold, T. Otto, J. Sauer, Alternative liquid fuels from renewable resources, Chemie Ingenieur Technik 90 (1–2) (2018) 99–112, https://doi.org/10.1002/cite.201700117.

[25] M.C. Zimmermann, T.N. Otto, S. Wodarz, T.A. Zevaco, S. Pitter, Mesoporous H–ZSM–5 for the conversion of dimethyl ether to hydrocarbons, Chemie Ingenieur Technik 91 (9) (2019) 1302–1313, https://doi.org/10.1002/cite.201800217.

[26] C.A. Farberow, S. Cheah, S. Kim, J.T. Miller, J.R. Gallagher, J.E. Hensley, J.A. Schaidle, D.A. Ruddy, Exploring Low-temperature dehydrogenation at ionic Cu sites in beta zeolite to enable alkane recycle in dimethyl ether homologation, ACS Catal. 7 (5) (2017) 3662–3667, https://doi.org/10.1021/acscatal.6b03582.

[27] Deutsches Institut für Normung, DIN EN ISO 3405:2019-09, Mineralölerzeugnisse und verwandte Produkte mit natürlichem oder synthetischem Ursprung - Bestimmung des Destillationsverlaufes bei Atmosphärendruck (ISO 3405:2019); Deutsche Fassung EN ISO 3405, (2019), https://doi.org/10.31030/3025519.

[28] Deutsches Institut für Normung, DIN EN 228:2017-08, Kraftstoffe - Unverbleite Ottokraftstoffe - Anforderungen und Prüfverfahren; Deutsche Fassung EN 228:2012+A1, (2017), https://doi.org/10.31030/2669458.

[29] X. Wang, M.A. Grose, R. Caldow, B.L. Osmondson, J.J. Swanson, J.C. Chow, J.G. Watson, D.B. Kittelson, Y. Li, J. Xue, H. Jung, S. Hu, Improvement of Engine Exhaust Particle Sizer (EEPS) size distribution measurement – II. Engine exhaust particles, J. Aerosol Sci. 92 (2016) 83–94, https://doi.org/10.1016/j.jaerosci.2015.11.003.

[30] TSI Incorporated, F. Rivision (Ed.), Model 3090 Engine Exhaust Particle Sizer Spectrometer Operation and Service Manual, 2009.

[31] Matter Engineering AG, B. Rivision (Ed.), Model 379020A Rotating Disk Thermodiluter and Model 379030 Thermal Conditioner Air Supply Operation and Service Manual, 2009.

[32] I. Abdul-Khalek, D. Kittelson, F. Brear, The influence of dilution conditions on diesel exhaust particle size distribution measurements, SAE Technical Paper Series, SAE Technical Paper Series, SAE International400 Commonwealth Drive, Warrendale, PA, United States, 1999, https://doi.org/10.4271/1999-01-1142.

[33] M. Bertsch, Experimental Investigations on Particle Number Emissions from GDI Engines, Dissertation Karlsruher Institut für Technologie, Karlsruhe, 2016, https://doi.org/10.5445/IR/1000063994.

[34] Control Sistem S.r.l, PSS-20 Manual, (2008).

[35] W.C. Hinds, Aerosol Technology: Properties, Behavior, and Measurement of Airborne Particles, 2nd edition, A Wiley-Interscience Publication, Wiley, New York, 1999http://www.loc.gov/catdir/description/wiley031/98023683.html.

[36] T. Michler, J. Dörnhöfer, D. Erforth, A. Heinz, K. Scheiber, P. Weber, N. Nowak, H. Kubach, J. Meyer, T. Koch, A. Dittler, Comparison of different particle measurement techniques at a heavy-duty diesel engine test bed, SAE Technical Paper Series, SAE Technical Paper Series, SAE International400 Commonwealth Drive, Warrendale, PA, United States, 2019, https://doi.org/10.4271/2019-24-0158.

[37] DEWESoft Measurement Innovation, Combustion analyser, http://www.dewesoft.com, (2015).

[38] J.B. Heywood, Internal Combustion Engine Fundamentals, second edition, Mechanical Engineering, 2018.

[39] A.E. Hassaneen, S. Samuel, I. Whelan, Combustion instabilities and nanoparticles emission fluctuations in GDI spark ignition engine, Int. J. Automot. Technol. 12 (6) (2011) 787–794, https://doi.org/10.1007/s12239-011-0091-z.

[40] D.P. Towers, C.E. Towers, Cyclic variability measurements of in-cylinder engine flows using high-speed particle image velocimetry, Measurement Science and Technology 15 (9) (2004) 1917–1925, https://doi.org/10.1088/0957-0233/15/9/032 (URL doi:10.1088/0957-0233/15/9/032).

[41] X. Yu, H. Wu, Y. Du, Y. Tang, L. Liu, R. Niu, R esearch on cycle-by-cycle variations of an SI engine with hydrogen direct injection under lean burn conditions, Applied Thermal Engineering 109 (2016) 569–581, https://doi.org/10.1016/j.applthermaleng.2016.08.077 http://www.sciencedirect.com/science/article/pii/S1359431116314363.

[42] C. Forte, E. Corti, G.M. Bianchi, S. Falfari, S. Fantoni, A RANS CFD 3D methodology for the evaluation of the effects of cycle by cycle variation on knock tendency of a high performance spark ignition engine, SAE Technical Paper Series, SAE Technical Paper Series, SAE International400 Commonwealth Drive, Warrendale, PA, United States, 2014, https://doi.org/10.4271/2014-01-1223.

[43] W.-D. Hsieh, R.-H. Chen, T.-L. Wu, T.-H. Lin, Engine performance and pollutant emission of an SI engine using ethanol–gasoline blended fuels, Atmospheric Environment 36 (3) (2002) 403–410, https://doi.org/10.1016/S1352-2310(01)00508-8 http://www.sciencedirect.com/science/article/pii/S1352231001005088.

[44] M. Al-Hasan, E ffect of ethanol–unleaded gasoline blends on engine performance and exhaust emission, Energy Convers. Manag. 44 (9) (2003) 1547–1561, https://doi.org/10.1016/S0196-8904(02)00166-8 http://www.sciencedirect.com/science/article/pii/S0196890402001668.

[45] J. Badra, A.S. AlRamadan, S.M. Sarathy, Optimization of the octane response of gasoline/ethanol blends, Applied Energy 203 (2017) 778–793, https://doi.org/10.1016/j.apenergy.2017.06.084 http://www.sciencedirect.com/science/article/pii/S030626191730836X.

[46] A. Demirbas, M.A. Balubaid, A.M. Basahel, W. Ahmad, M.H. Sheikh, Octane rating of gasoline and octane booster additives, Pet. Sci. Technol. 33 (11) (2015) 1190–1197, https://doi.org/10.1080/10916466.2015.1050506.

[47] H. Portz, Brand- und Explosionsschutz von A-Z: Begriffserläuterungen und brandschutztechnische Kennwerte, Vieweg+Teubner Verlag, Wiesbaden, 2005, https://doi.org/10.1007/978-3-322-80197-5. URL http://gbv.eblib.com/patron/FullRecord.aspx?p=1998358.

[48] P. Helmetsberger, Experimentelle Gemischbildungsuntersuchungen an einem Ottomotor mit vollvariablem Ventiltrieb, Direkteinspritzung und Aufladung,

Dissertation Technischen Universität Graz, Graz, 2010https://diglib.tugraz.at/download.php?id=576a7a8175fdflocation=browse.
[49] P. Sementa, B. Maria Vaglieco, F. Catapano, Thermodynamic and optical characterizations of a high performance GDI engine operating in homogeneous and stratified charge mixture conditions fueled with gasoline and bio-ethanol, Fuel 96 (2012) 204–219, https://doi.org/10.1016/j.fuel.2011.12.068 http://www.sciencedirect.com/science/article/pii/S0016236111008490.
[50] H. Dageförde, Untersuchung innermotorischer Einflussgrößen auf die Partikelemission eines Ottomotors mit Direkteinspritzung. doi:https://doi.org/10.5445/IR/1000049421.
[51] M. Bertsch, T. Koch, A. Velji, Influence of charge motion and injection pressure on the particulate emission of a gasoline DI-SI engine at homogeneous, boosted operation, SIA-Société des ingénieurs de lautomobile (ed.), SIA Powertrain: the low CO2 Spark Ignition Engine the Low CO2 Spark Ignition Engine of the Future and its Hybridization, Versailles.
[52] D. Notheis, M. Bertsch, A. Velji, T. Koch, Investigations on PN formation and emission from passenger car GDI engines, 18. Internationales Stuttgarter Symposium, 2018, pp. 1041–1055.
[53] Y. Kim, Y. Kim, J. Kang, S. Jun, S. Rew, D. Lee, S. Park, Fuel effect on particle emissions of a direct injection engine, SAE Technical Paper Series, SAE Technical Paper Series, SAE International400 Commonwealth Drive, Warrendale, PA, United States, 2013, https://doi.org/10.4271/2013-01-1559.
[54] M.A. Ratcliff, J. Burton, P. Sindler, E. Christensen, L. Fouts, G.M. Chupka, R.L. McCormick, Knock resistance and fine particle emissions for several biomass-derived oxygenates in a direct-injection spark-ignition engine, SAE International Journal of Fuels and Lubricants 9 (1) (2016) 59–70, https://doi.org/10.4271/2016-01-0705.
[55] L. de Francquevillle, G. Pilla, Investigation of particle formation processes in a GDI engine in catalyst heating operation, SIA Conference-the Spark Ignition Engine of the Future, Strasbourg, France, 2011.
[56] W. Wiese, C. Laidig, E. Schünemann, F. Balthasar, J. Cahal, Effects of fuel composition, additives and injection parameters on particulate formation of gasoline di engines, 39. Internationales Wiener Motorensymposium, Wien, 2018.
[57] D. Tanaka, R. Uchida, T. Noda, A. Kolbeck, S. Henkel, Y. Hardalupas, A. Taylor, A. Aradi, Effects of Fuel properties associated with in-cylinder behavior on particulate number from a direct injection gasoline engine, in: SAE Technical Paper Series, SAE Technical Paper Series, SAE International400 Commonwealth Drive, Warrendale, PA, United States, 2017. doi:https://doi.org/10.4271/2017-01-1002.
[58] S. Di Iorio, M. Lazzaro, P. Sementa, B.M. Vaglieco, F. Catapano, Use of renewable oxygenated fuels in order to reduce particle emissions from a GDI high performance engine, SAE Technical Paper Series, SAE Technical Paper Series, SAE International400 Commonwealth Drive, Warrendale, PA, United States, 2011, https://doi.org/10.4271/2011-01-0628.
[59] M. Fatouraie, M. Frommherz, M. Mosburger, E. Chapman, S. Li, R. McCormick, G. Fioroni, Investigation of the impact of fuel properties on particulate number emission of a modern gasoline direct injection engine, SAE Technical Paper Series, SAE Technical Paper Series, SAE International400 Commonwealth Drive, Warrendale, PA, United States, 2018, https://doi.org/10.4271/2018-01-0358.
[60] T. Tahtouh, A. Ben Amara, P. Anselmi, L. Starck, Impact of ethanol and aromatic hydrocarbons on particulate emissions from a gasoline vehicle, SAE Technical Paper Series, SAE Technical Paper Series, SAE International400 Commonwealth Drive, Warrendale, PA, United States, 2019, https://doi.org/10.4271/2019-24-0160.
[61] G. Karavalakis, D. Short, D. Vu, R. Russell, M. Hajbabaei, A. Asa-Awuku, T.D. Durbin, Evaluating the effects of aromatics content in gasoline on gaseous and particulate matter emissions from SI-PFI and SIDI vehicles, Environmental Science & Technology 49 (11) (2015) 7021–7031, https://doi.org/10.1021/es5061726.
[62] M. Raza, L. Chen, F. Leach, S. Ding, A review of particulate number (PN) emissions from gasoline direct injection (GDI) engines and their control techniques, Energies 11 (6) (2018) 1417, https://doi.org/10.3390/en11061417.
[63] J. Czerwinski, P. Comte, N. Heeb, A. Mayer, V. Hensel, Nanoparticle Emissions of DI gasoline cars with/without GPF, in: SAE Technical Paper Series, SAE Technical Paper Series, SAE International400 Commonwealth Drive, Warrendale, PA, United States, 2017. doi:https://doi.org/10.4271/2017-01-1004.
[64] X. Liu, T. Chanko, C. Lambert, M. Maricq, Gasoline particulate filter efficiency and backpressure at very low mileage, SAE Technical Paper Series, SAE Technical Paper Series, SAE International400 Commonwealth Drive, Warrendale, PA, United States, 2018, https://doi.org/10.4271/2018-01-1259.
[65] C.-L. Myung, J. Kim, W. Jang, D. Jin, S. Park, J. Lee, Nanoparticle filtration characteristics of advanced metal foam media for a spark ignition direct injection engine in steady engine operating conditions and vehicle test modes, Energies 8 (3) (2015) 1865–1881, https://doi.org/10.3390/en8031865.
[66] A. Massner, U. Gärtner, T. Koch, Die Reaktivität von Dieselruß und die Auswirkungen auf den Betrieb von Abgasnachbehandlungssystemen, 9. FAD Konferenz, Dresden, 2011.
[67] H. Bladt, Oxidationsreaktivität von Rußen: Einfluss intern gemischter Mineralien sowie Kraftstoff- und Abgaszusammensetzung, Dissertation, Technische Universität München, München.
[68] S. Lindner, Rußreaktivität bei Nutzfahrzeugdieselmotoren, Dissertation Karlsruher Institut für Technologie, Karlsruhe, 2016, https://doi.org/10.5445/IR/1000059601.
[69] H. Zhang, W.-X. Pu, S. Ha, Y. Li, M. Sun, The influence of included minerals on the intrinsic reactivity of chars prepared at 900°C in a drop tube furnace and a muffle furnace, Fuel 88 (11) (2009) 2303–2310, https://doi.org/10.1016/j.fuel.2009.05.014.
[70] A. Zolin, A.D. Jensen, P.A. Jensen, K. Dam-Johansen, Experimental study of char thermal deactivation, Fuel 81 (8) (2002) 1065–1075, https://doi.org/10.1016/S0016-2361(02)00009-1.
[71] C. Wang, H. Xu, J.M. Herreros, T. Lattimore, S. Shuai, Fuel effect on particulate matter composition and soot oxidation in a direct-injection spark ignition (DISI) engine, Energy Fuel 28 (3) (2014) 2003–2012, https://doi.org/10.1021/ef402234z.
[72] A.R. Chughtai, J.M. Kim, D.M. Smith, The effect of air/fuel ratio on properties and reactivity of combustion soots, Journal of Atmospheric Chemistry 43 (1) (2002) 21–43, https://doi.org/10.1023/A:1016131112199 (URL doi:10.1023/A:1016131112199).
[73] D.S. Su, J.-O. Müller, R.E. Jentoft, D. Rothe, E. Jacob, R. Schlögl, Fullerene-like soot from EuroIV diesel engine: consequences for catalytic automotive pollution control, Top. Catal. 30 (1) (2004) 241–245, https://doi.org/10.1023/B:TOCA.0000029756.50941.02.
[74] R.L. Vander Wal, A.J. Tomasek, Soot oxidation: dependence upon initial nanostructure, Combustion and Flame 134 (1) (2003) 1–9, https://doi.org/10.1016/S0010-2180(03)00084-1 http://www.sciencedirect.com/science/article/pii/S0010218003000841.
[75] K. Yehliu, R.L. Vander Wal, O. Armas, A.L. Boehman, Impact of fuel formulation on the nanostructure and reactivity of diesel soot, Combustion and Flame 159 (12) (2012) 3597–3606, https://doi.org/10.1016/j.combustflame.2012.07.004 http://www.sciencedirect.com/science/article/pii/S0010218012002052.
[76] N. Bock, J. Jeon, D. Kittelson, W. Northrop, Effects of fuel properties on particle number and particle mass emissions from lean and stoichiometric gasoline direct injection engine operation, SAE Technical Paper Series, SAE Technical Paper Series, SAE International400 Commonwealth Drive, Warrendale, PA, United States, 2019, https://doi.org/10.4271/2019-01-1183.
[77] T. Thummadetsak, A. Wuttimongkolchai, S. Tunyapisetsak, T. Kimura, Effect of gasoline compositions and properties on tailpipe emissions of currently existing vehicles in Thailand, SAE Technical Paper Series, SAE Technical Paper Series, SAE International400 Commonwealth Drive, Warrendale, PA, United States, 1999, https://doi.org/10.4271/1999-01-3570.
[78] Y.-C. Yao, J.-H. Tsai, A.-L. Chang, F.-T. Jeng, E ffects of sulfur and aromatic contents in gasoline on motorcycle emissions, Atmos. Environ. 42 (26) (2008) 6560–6564, https://doi.org/10.1016/j.atmosenv.2008.04.031 http://www.sciencedirect.com/science/article/pii/S1352231008004846.
[79] R. Brown, J.L. York, Sprays formed by flashing liquid jets, AICHE J. 8 (2) (1962) 149–153, https://doi.org/10.1002/aic.690080204.
[80] M. Mojtabi, G. Wigley, J. Helie, The effect of flash boiling on the atomization performance of gasoline direct injection multistream injectors, Atomization and Sprays 24 (6) (2014) 467–493, https://doi.org/10.1615/AtomizSpr.2014008296.